Journal of Cultural Heritage 57 (2022) 154–164

Contents lists available at ScienceDirect

Journal of Cultural Heritage

journal homepage: www.elsevier.com/locate/culher

VSI: Geomaterials in CH

Recession rate of carbonate rocks used in cultural heritage: Textural control assessed by accelerated ageing tests

Silvia Salvini[a,b], Renzo Bertoncello[c], Chiara Coletti[a], Luigi Germinario[a], Lara Maritan[a], Matteo Massironi[a], Riccardo Pozzobon[a], Claudio Mazzoli[a,*]

[a] Department of Geosciences, University of Padova, Padova, Italy
[b] Italian Ministry of Culture, Gallerie dell'Accademia di Venezia, Cannaregio 3553, Venice, Italy
[c] Department of Chemical Sciences, University of Padova, Padova, Italy

ARTICLE INFO

Article history:
Received 2 April 2022
Accepted 12 August 2022
Available online 26 August 2022

Keywords:
Recession rate
Ageing tests
Rainwater simulation
Confocal microscopy
Grain-size
Carbonate rocks

ABSTRACT

In this study, the recession rate of eleven carbonate stones widely used in the cultural heritage of north-eastern Italy and differing in their textural features and mineralogical composition was investigated. Samples of stones known as Vicenza (Nanto and Costozza varieties), Carrara marble, Verona (Red and Brown varieties), Asiago, Istria (Orsera variety), Aurisina, Chiampo (Ondagata and Paglierino varieties), and Botticino were subjected to accelerated ageing tests in an environmental test chamber for simulating the effect of rainfall, using two different water compositions corresponding to rainwater chemistry in the cities of Bologna (pH ~ 7) and Stresa (pH ~ 6) in Italy. Bulk stone recession was evaluated considering sample weight loss as a function of the number of wetting cycles. Moreover, direct measurements of recession were performed by confocal microscopy, which allowed 3D surface reconstruction of the stone surface and evaluation of differential recession as a function of calcite grain size. The results also allowed the definition of correction coefficients for calculating more precisely the recession rate of carbonate rocks using known recession equations from the literature. This pilot study illustrates a rapid and efficient methodological approach that can be used for providing reliable estimates of future stone deterioration in cultural heritage, related to specific environmental conditions and expected climate scenarios, which can be exploited for evaluating risk-based protection measures of a variety of historical artifacts and structures.

© 2022 The Authors. Published by Elsevier Masson SAS.
This is an open access article under the CC BY-NC-ND license
(http://creativecommons.org/licenses/by-nc-nd/4.0/)

1. Introduction

Water is a first-order driving force for stone damage, because it interacts in various ways with the material causing different decay patterns. The direct or indirect presence of water in the solid, liquid, or gaseous state influences various largely studied chemical and physical processes, including ice crystallization [1–6], salt crystallization [7–19], vapour condensation and evaporation [20–22], biodeterioration [23–27], and dissolution.

The main theme of this paper is related to stone dissolution caused by the interaction with rainwater. That is a complex process, enhanced by the introduction into the atmosphere of anthropogenic pollutants from different sources, such as power plants, domestic heating, automotive and air transport, etc.; the relevant emissions are associated with the increased atmospheric concentration of inorganic and organic compounds in the form of gases, aerosols and particulate matter, which cause rainwater acidification. The potential threat of acid rain to cultural heritage, especially to the assets made of carbonate rocks, is widely studied in the literature and is a major concern in conservation science [28–36].

When a carbonate rock is exposed to rainwater, different chemical reactions take place [37–39]: dissolution in clean rain or "karst effect" [29,40,41]; accelerated dissolution in acid rain; dry deposition [42,43]. Moreover, gaseous components of the atmosphere, such as SO_2, SO_3, NO_x, O_3, Cl_2, and organic oxidants, partially dissolve in rainwater, increasing its acidity, while rain droplets capture soot and larger molecules during precipitation, carrying them to the ground or stone surface and causing the formation of black crusts and whitening [44–47]. Although small quantities of sulfates, nitrates, and chlorides are supplied by natural sources, the

* Corresponding author.
E-mail address: claudio.mazzoli@unipd.it (C. Mazzoli).

https://doi.org/10.1016/j.culher.2022.08.010
1296-2074/© 2022 The Authors. Published by Elsevier Masson SAS. This is an open access article under the CC BY-NC-ND license
(http://creativecommons.org/licenses/by-nc-nd/4.0/)

majority is introduced into the atmosphere by human activities. In addition to NO_x and SO_2, the combustion of fossil fuels produces large quantities of CO_2, CO, soot, and polycyclic aromatic hydrocarbons [48–52].

The effects of pollutant concentration in the atmosphere, rainfall, and air temperature are described in terms of damage functions, and the decay phenomena of stone materials are quantified by considering changes in their surface topography, being either loss of material, or surface recession. Several studies [57–66] tried to assess the contribution of different processes to the overall stone decay and estimate its rate. Numerous equations have been drafted and, amongst them, Lipfert's equation [41] is the most commonly used:

$$\frac{\text{loss } (\mu\text{m})}{\text{rain (m)}} = 18.8 + 0.016\ [H^+] + 0.18(Vd_S * [SO_2] + Vd_N * [HNO_3])/R$$

where $[H^+]$ is the concentration of hydrogen ions in rainwater in nmol/cm^2·s, Vd_S and Vd_N are the deposition velocities of SO_2 and HNO_3 in cm/s, $[SO_2]$ and $[HNO_3]$ are the SO_2 and HNO_3 concentrations in the atmosphere in µg/m^3, and R is the annual precipitation in m. The term "Vd_N * $[HNO_3]$" is often omitted, assuming that its contribution to recession rate is negligible. The intercept value of 18.8 derives from the solubility of calcite in equilibrium with 330 ppm of CO_2 in the atmosphere. This relation returns an average (generally annual) recession rate, with the other parameters averaged over the period of interest. Lipfert's function has been taken into consideration to quantify the annual surface recession of carbonate stones, and some authors applied it for predicting future limestone recession over long periods of time [6,53], under different IPCC scenarios of climate change in Europe [38]. Accordingly, patterns of erosion rate of heritage materials were predicted in urban areas and across wide regions [54,55]. Other authors rearranged Lipfert's damage function in order to reconstruct past atmospheric SO_2 pollution levels from recession rate measurements [56].

A similar equation was proposed by Reddy and co-authors [57] to evaluate the annual surface recession normalized to annual rainfall:

$$\frac{\text{loss } (\mu\text{m})}{\text{rain (m)}} = 4.88 + 150\frac{[H^+]}{R} + 0.069\ SO_2$$

where SO_2 concentration is expressed as µg/m^3 and $[H^+]$ in mmol/L.

Baedecker [58] designed another recession equation based on the combined effect of temperature and concentration of hydrogen ions on material loss:

$$\frac{\text{mmol } Ca^{2+}}{\text{L}} = 0.16\left[1.0 - 0.015\ T + 0.0000922\ T^2\right]/0.683 + 0.49\left[H^+\right]$$

where T is temperature in °C, and $[H^+]$ is expressed in mmol/L. Having material loss measured in mmol/L of Ca^{2+} ions is not so immediate. For this reason, Delalieux and co-authors [59] modified the mathematical formulation considering linear recession in µm instead:

$$\frac{\text{loss } (\mu\text{m})}{\text{rain (m)}} = 9.4 * \left[1.0 - 0.015\ T + 0.000092\ T^2\right] + 20\left[H^+\right].$$

It is also worth mentioning the equation proposed by Webb and co-authors [60], which considers the concentration of various pollutants expressed in ppb/day, R (rainfall) expressed in mm/day, acid ionic concentration in mol/m^2, and the material weight loss per unit of surface:

$$\frac{g}{m^2} = -0.162 + 0.0058\ SO_2 + 0.0666\ R + 638\ \text{acid} - 0.026\ NO_2 + 0.0155\ NO + 0.0007\ O_3.$$

This equation was also adjusted by Delalieux and co-authors [59], in order to express material loss of carbonate rocks as linear surface recession (µm), using a general density value of limestones (2500 kg/m^3) and converting daily values in annual averages:

$$\frac{\text{loss } (\mu\text{m})}{\text{rain (m)}} = \frac{150}{R} * \left(-0.16 + 0.0020\ SO_2 + 0.18\ R + 1.7\left[H^+\right] * R - 0.0013\ NO_2 + 0.0086\ NO + 0.0003\ O_3\right)$$

where the concentration of SO_2, NO_2, NO and O_3 is expressed in µg/m^3, $[H^+]$ in mmol/L, R (rainfall) in m/year.

Kucera and Fitz [61] derived their equation based on run-off tests, which lasted four years. Below is their formulation of total material loss expressed in g/m^2:

$$\frac{g}{m^2} = 34.4 + 5.96\ [TOW] * SO_2 + 388\ R * [H^+]$$

where TOW is the time of wetting (period of time when relative humidity is higher than 80% and temperature is above 0 °C), SO_2 concentration is expressed in µg/m^3, $[H^+]$ in mg/L, and R (rainfall) in m/year. This expression was also rearranged with the same units as previously described [59]:

$$\frac{\text{loss } (\mu\text{m})}{\text{rain (m)}} = \frac{0.1}{R} * (34 + 6.0[TOW] * SO_2 + 390\left[H^+\right] * R).$$

Kucera and co-authors [64] investigated the effect of the contemporaneous occurrence of different pollutants on materials, including cultural heritage, in the frame of international exposure programs [62,63], and proposed the following damage function for carbonate rocks:

$$\text{loss } (\mu\text{m}) = 3.95 + 0.0059\ SO_2 * RH_{60} + 0.054\ R\left[H^+\right] + 0.078\ HNO_3 * RH_{60} + 0.0258\ PM_{10}$$

where SO_2, HNO_3, and PM_{10} concentration is expressed in µg/m^3, $[H^+]$ in mg/L (possible range: 0.0006–0.13), R (rainfall) in mm, and RH_{60} is the measured relative humidity when it is above 60% (otherwise a null value is assigned).

A further attempt to describe stone damage is found in Delalieux and co-authors [59]:

$$\frac{\text{loss } (\mu\text{m})}{\text{rain (m)}} = \frac{0.015}{R} * (-29 + 590R + 800\ [H^+] * R + 5300\ [SO_4^{2-}] * R + 5.5\ SO_2)$$

where R (rainfall) is expressed in m/year, SO_2 concentration in µg/m^3, and $[H^+]$ and $[SO_4^{2-}]$ are ionic concentrations in rainwater expressed in mmol/L.

Lan and co-authors [65] accounted for the effect of stone exposure to sheltered and unsheltered environments after a number of field experiments, obtaining the following damage function in sheltered areas:

$$\text{loss } (\mu\text{m}) = (0.00111\ RH * SO_2) * t^{\ 0.784}$$

whereas, in unsheltered areas, the recession resulted to be described by the following expression:

$$\text{loss } (\mu\text{m}) = (0.00233\ RH * SO_2) * t + 0.00309\ R$$

where R (rainfall) is expressed in mm, t is the exposure time in years, SO_2 concentration is expressed in ppb, and RH is the average relative humidity in%.

Finally, Livingston [66] applied an aqueous geochemical modelling approach to determine the effect of acid rain runoff and dry deposition on carbonate dissolution. The author calculated the acid

neutralization path in the pH range 3.5–6 and the effect of dry deposition, describing material loss in terms of amount of Ca^{2+} ions released, applying the electroneutrality condition between the solution chemistry of rainfall and runoff:

$$\Delta\ Ca^{2+} = \Delta\ SO_4^{2-} + 0.5\ \Delta\ NO_3^- + 0.5\ \Delta\ \left(Cl^- - Na^+\right) + 0.5\ \Delta\ Alk\ +\ \Delta\ Organics.$$

where "Alk" indicates an alkalinity function (HCO_3^- – H^+) and "Organics" indicate the content in organic acids. Livingston [66] concluded that dry deposition has the potential to contribute to carbonate dissolution nearly by an order of magnitude more than wet acid neutralization.

Many scientists have focused their attention on the field test method in order to overpass the variability of rainwater composition and observe the decay of different stones in the same natural environment or of the same stone in different environments and locations [67]. Nevertheless, field tests present various issues: (i) the rate of stone decay is relatively slow compared to the standard timings required by a scientific research project to achieve its final results, thus, the quantification of the environmental parameters is affected by considerable errors; (ii) realistic exposure tests should be designed for much longer periods, at least ten years, in order to obtain meaningful recession estimates [68,69]; (iii) the results on stone recession obtained at a specific site are hardly applicable elsewhere. Indeed, real situations are often extremely complex (various sources of pollution, orientation with respect to the geographical coordinates, extreme acid rain events, wind-blown dust, wind-blown marine aerosols, temperature and relative humidity regime, volcanic emissions, etc.); therefore, the combination of deterioration factors is hardly similar in different localities unless in terms of generic climate conditions, which may determine what deterioration mechanisms tend to prevail [70,71].

Some authors tried to reduce the number of variables, for example simplifying rainwater composition [29,72], or reproducing as closely as possible the chemical characteristics of natural rainfall [73], or using environmental test chambers. The latter is a widespread practice in conservation science for testing material decay and conservation products under specified environmental conditions [74–77].

Other works developed different approaches, e.g., comparing photographs taken at different times [78,79], measuring with micrometers the variations in elevation with respect to a reference surface [68,69,80], determining the surface recession of slabs or headstones using calipers [81–84] or by measuring the height difference between the lead lettering and the marble surface [85], quantifying the Ca^{2+} ions leached from the surface during runoff experiments [59,86].

Comparing the large differences between the theoretical dose-response functions and the direct measurements of stone erosion found in the literature, a non-linear response of recession rate to environmental changes can be often observed [87–92]. Large discrepancies arose when damage functions were tested against long-term (over decadal) direct recession measurements, leading to unacceptable underestimations of surface erosion rate [68,69].

2. Research aims and contributions

The models of surface recession rate for carbonate rocks need a reformulated equation in order to obtain reliable durability predictions in a climate change scenario, especially in view of the potential impact on the weathering and conservation of heritage sites and monuments made of stone and the increased risk to their survival and proper management. In particular, additional factors that have a first-order effect on deterioration need to be considered, namely the petrographic features, i.e., the mineralogical composition and texture (porosity, grain size, etc.). These properties and their effects were evaluated in the present research while measuring the recession rate of stones exposed to cycles of immersion and emersion (wet-dry) in an environmental test chamber. The cycles were conducted using two different types of water, artificially prepared in order to be as similar as possible to the rainwater in the northern Italy cities of Bologna [93] and Stresa [94], with pH ∼ 7, and ∼ 6, respectively.

3. Materials and methods

3.1. Material selection

The materials to be subjected to the accelerated ageing tests were selected amongst those most frequently used in the built environment of northeastern Italy. Eleven carbonate rock types (Table 1) were chosen, covering a large range of petrographic and textural features. In particular, Carrara marble was included because most of the previous studies on the recession rate of carbonate rocks are mainly based on measurements performed on that or other marbles [81,84].

The usage of the selected stones covers millennia of history and often goes well beyond the regional borders of the respective quarry areas, even involving a number of UNESCO World Heritage Sites.

The most renowned stone is Carrara marble, whose usage by architects and sculptors can be admired worldwide, with the most celebrated examples being probably in Italy and including, amongst others, the Pantheon in Rome from the Roman Age, the complex of Florence Cathedral from the Middle Ages, and Michelangelo's Pietà and David from the Renaissance. Focusing on northeastern Italy, the stones from Istria and Verona were likewise exploited by the Romans, but their fortune is bond to the works commissioned by the Republic of Venice *Serenissima* in its large territories spanning from Italy to the Balkans: for instance, in Venice, Istria stone can be observed in Rialto Bridge, the Bridge of Sighs, and the Doge's Palace, and architectural elements and details in Verona stone can be seen in St. Mark's Basilica, Ca' d'Oro, and the Doge's Palace again. With regard to Botticino, this material has found a wide application nearby the city of Brescia (in Roman temples and theaters, churches, palaces, etc.), but from the end of the 19th century it was commercialized in the rest of Italy and abroad: it has been used in the Vittoriano monument in Rome and the White House of Washington in the USA, just to name a few examples.

The other materials selected are probably less famous and their applications are mostly local, although still keeping a relevance in the national and, in some cases, international market. Vicenza stone was particularly appreciated by the Renaissance architect Palladio, who used it in his Olympic theater, Basilica Palladiana, and the villas in Vicenza. Finally, the stones of Chiampo, Aurisina, and Asiago have been used especially for historical construction in the Veneto region and, more generally, in northern Italy.

3.2. Petrographic analysis

Thin sections were observed using a Zeiss® Axio Scope.A1 polarized-light optical microscope (OM) coupled with an Axio CamMRC5 in order to determine their petrographic and textural features.

The mineralogical composition was identified by X-Ray Powder Diffraction (XRPD) using a PANalytical θ-θ diffractometer equipped with a Cu X-ray tube operating at 40 kV and 40 mA, a sample spinner, a Ni filter and a solid-state detector (X'Celerator). The semi-quantitative analysis was performed with the Reference Intensity Ratio (RIR) method.

Table 1
Summary of the petrographic classification, geological formation, and sedimentation age of the carbonate rocks considered in this research.

Stone ID	Commercial name	Rock type	Geological Formation	Sedimentation Age
NA	Nanto Stone	Packstone/Rudstone	Nummulitic Limestone Formation	Early-Middle Eocene
CO	Costozza Stone	Grainstone/Rudstone	Castelgomberto Limestone Formation	Oligocene
AU	Aurisina Stone	Rudstone/Grainstone	Sežana and Lipica Formations	Late Cretaceous
OR	Orsera Stone	Mudstone	Kirmenjak Unit	Late Tithonian
PA	Chiampo Paglierino Stone	Rudstone	Nummulitic Limestone Formation	Early-Middle Eocene
ON	Chiampo Ondagata Stone	Rudstone	Nummulitic Limestone Formation	Early-Middle Eocene
RV	Red Verona Stone	Wackestone	Rosso Ammonitico Veronese Formation	Middle-Late Jurassic
BV	Brown Verona Stone	Wackestone	Rosso Ammonitico Veronese Formation	Middle-Late Jurassic
RO	Pink Asiago Stone	Mudstone/Wackestone	Maiolica Formation	Early Cretaceous
BO	Botticino Stone	Floatstone/Crystalline carbonate	Corna Formation	Early Jurassic
M	Carrara Marble	Marble	Tuscan Nappe	Early Jurassic

Mercury intrusion porosimetry (MIP) was performed using a PoreMaster 33 system (Quantachrome Instruments ®) with the following parameters: sample cell is 1.0 × 3.0 cm in size and 2 cm^3 in volume, pressure range is 0.5–33.000 psi, contact angle (θ) of mercury is 140, surface tension (σ) of mercury is 0.48 N/m (480 dyn/cm), and pore size range is from 0.0064 to 950 µm. True density of the materials was measured through a picnometer Ultrapyc 1200. The considered density value is the mean of 10 measures.

3.3. Sample preparation for the ageing tests

One sample for each of the eleven rock types selected (size ~ 2 × 2 × 1 cm) was prepared to be subjected to accelerated ageing tests in an environmental test chamber. Stainless steel washers were cut in two halves and attached to the opposite sides of each specimen with Araldite 2020. These metal parts are resistant to decay, and therefore can be used as a reference surface in the evaluation of stone recession. The sample surface was polished on sandpaper with a grit of 1200.

3.4. Water preparation for the ageing tests

The accelerating ageing tests consisted in a sequence of immersion and emersion cycles in two different aqueous solutions artificially prepared to be as similar as possible to the rainwater in the city of Bologna [93], with a pH ~ 7, and Stresa [94], with a pH ~ 6. These two locations were chosen since no other detailed measurement of rainwater composition in Italian cities was found in the peer-reviewed literature. The ionic concentrations (in mmol/45 l, where 45 l is the total volume of the water to be put inside the environmental test chamber) of these two types of water are: 1.575 (Na^+), 0.495 (K^+), 0.540 (Mg^{2+}) 3.465 (Ca^{2+}), 1.755 (Cl^-), 1.575 ($SO_4{}^{2-}$), and 4.23 ($HCO_3{}^-$) for the water of Bologna, and 0.810 (Na^+), 0.135 (K^+), 0.360 (Mg^{2+}), 2.88 (Ca^{2+}), 0.405 (Cl^-), 3.69 ($SO_4{}^{2-}$), 1.89 ($HCO_3{}^-$), 2.34 ($NH_4{}^+$), 1.80 ($NO_3{}^-$), and 0.675 (H^+) for the water of Stresa. The necessary ions were introduced in the form of the following compounds: $CaCO_3$, $CaCl_2$, KCO_3, Na_2SO_4, $Mg(OH)_2$, H_2SO_4(96%), NaCl, $CaSO_4$, $MgSO_4{\bullet}7H_2O$, $[NH_4]_2SO_4$, $[NH_4]NO_3$, KNO_3, NH_3(21%), HNO_3(98%).

3.5. Environmental test chamber

The ageing tests were performed using a benchtop environmental chamber Suntest CPS$^+$ equipped with a Xenon Arc Lamp and an immersion system to cover completely the specimens with water. The chamber tank can contain up to 45 liters of water. The instrument is also equipped with a parabolic reflector, a photodiode, and a ventilation system. The samples were subjected to 240 dry-wet cycles, each consisting of one immersion phase and one emersion phase. Each immersion phase lasted 60 min, with water temperature of 25 °C and under irradiation of 300 W/m^2, determining a reference surface temperature of 40 °C, followed by a 180 min emersion phase under irradiation of 500 W/m^2, determining a reference surface temperature of 70 °C.

3.6. Recession measurements

Material loss of the different specimens with respect to the original stone surface was measured after 54, 141, and 240 cycles. Stone surface recession was evaluated in different ways.

Table 2
Results of the laboratory analyses by XRD, MIP, densitometry, and average grain-size (expressed in microns) of different textural elements recognized and measured on thin section under the optical microscope. In brackets, the standard deviation (sd) is also reported. Specific surface area was calculated from MIP data using the Rootare-Prenzlow equation [97]. Botticino stone (BO) contains dolomite crystals with an average grain-size of 127 µm (sd = 51). Mineral abbreviations: Cal = calcite; Qz = quartz; Dol = dolomite, Mg-Cal=Mg-Calcite, Ms = muscovite; Ill = Illite; Plg M = palygorskyte M. Stone ID as in Table 1.

Stone ID	Mineralogical composition	MIP		True Density (g/cm^3)	Specific surf area (m^2/g)	Fine-grained micrite	Coarse-grained micrite	Sparite	Bioclast filling
		Porosity (vol%)	Max diameter (µm)						
NA	95% Cal, 5% Ill	27.18	371.77	2.789	2.2603	0.5 (1)	6.2 (2)	45 (4)	34 (10)
CO	100% Cal	28.52	221.52	2.737	1.769	0.5 (1)	–	38 (10)	32 (8)
AU	100% Cal	4.61	272.89	2.705	0.7515	0.5 (1)	3.5 (1.2)	30 (5)	21 (2)
OR	100% Cal	0.40	211.13	2.711	0.0002	0.2 (0.5)	–	40 (7.5)	–
PA	61% Cal, 38% Mg-Cal, 1% Plg M	0.36	221.52	2.708	0.4630	0.5 (1)	4.0 (6)	45 (7.5)	28 (7.5)
ON	66% Cal, 34% Mg-Cal, traces Plg M	1.04	216.47	2.707	0.0003	0.5 (1)	5.0 (2)	41 (5)	15 (4)
RV	100% Cal	0.26	379.47	2.729	0.1267	3.0 (1)	–	–	44 (10)
BV	94% Cal, 4% Ill, 2% Qtz	0.10	4.04	2.720	0.0000	1.0 (1)	5.0 (1)	24 (7.2)	28 (5)
RO	98% Cal, 2% Qz	3.54	216.47	2.688	3.3939	0.4 (1)	4.3 (1.7)	–	35 (6)
BO	57% Cal, 43% Dol	1.73	235.34	2.766	0.1496	2.0 (1)	6.1 (1.8)	–	14 (2)
M	100% Cal, traces Ms	1.00	215.56	2.741	0.0385	–	–	156 (100)	–

The first method consisted in the measurement of the sample weight loss using an analytical scale (accuracy 0.0001 g). Weight loss was calculated from the difference between the weight of the oven-dried samples before all the ageing cycles and the weight recorded after each step as above. All the measurements were done on oven-dried samples. Weight loss was then converted to volume loss dividing by stone density, and then to linear recession dividing by the sample area calculated from the dimensions measured with a calliper (accuracy 0.001 mm). This method has the advantage to be fast and precise in determining material loss, providing an estimate of the average surface recession, but fails to reveal possible differential recession of areas with different textural features (e.g. grain-size) and/or different mineralogy (e.g. calcite and dolomite).

The second method consisted in a three-dimensional surface mapping using a confocal laser microscope Olympus Lext OLS4000. For each sample, a matrix of 6 × 6 scans were acquired at a magnification of 200x. Each scan consisted of a number of acquisition layers merged by the LEXT acquisition software, the number of which strongly depends on the surface roughness of the samples and affects total acquisition time. Each acquisition resulted in a surface topographic map of about 3 × 3 mm, with a lateral resolution of 1 µm, and a submicrometric vertical resolution. For each sample four different topographic maps were produced, one before the ageing tests and one after each set of ageing cycles (i.e., after 54, 141, and 240 cycles). These data were then exported as comma-separated value (csv) files and processed with a Matlab® script that converts them into GIS-ready point clouds to be successively imported in into ArcMap® for further analysis [95]. For computational reasons, the point clouds were subsampled, reducing lateral resolution to 5 µm. For each of the topographic maps, a reference surface was constructed parallel to the sample surface taking the elevation of the metal anchoring plate as an absolute height reference. The recession in each specific point or subset of points within a selected area of interest (ROI) of the rock sample (e.g. a homogeneous micritic area, a bioclast, a sparitic domain) was then obtained from the elevation difference with the reference surface by subtracting the elevation difference obtained on the same area before the ageing tests. Hence, the average recession value of each sample was measured by averaging the relative elevation of all the points included in a ROI obtained by selecting almost the entire scanned area, thus including all the texturally different areas, each characterized by a different elevation.

This second method allows a direct measurement of the surface recession, revealing possible differences in recession of areas characterized by different textural features and/or mineralogy. The disadvantage of this approach is that the area investigated is necessarily limited, thus it is less precise in the estimation of the average recession, especially in texturally heterogeneous rocks. Therefore, it is important to wisely select an area that represents the different textural elements of the sample.

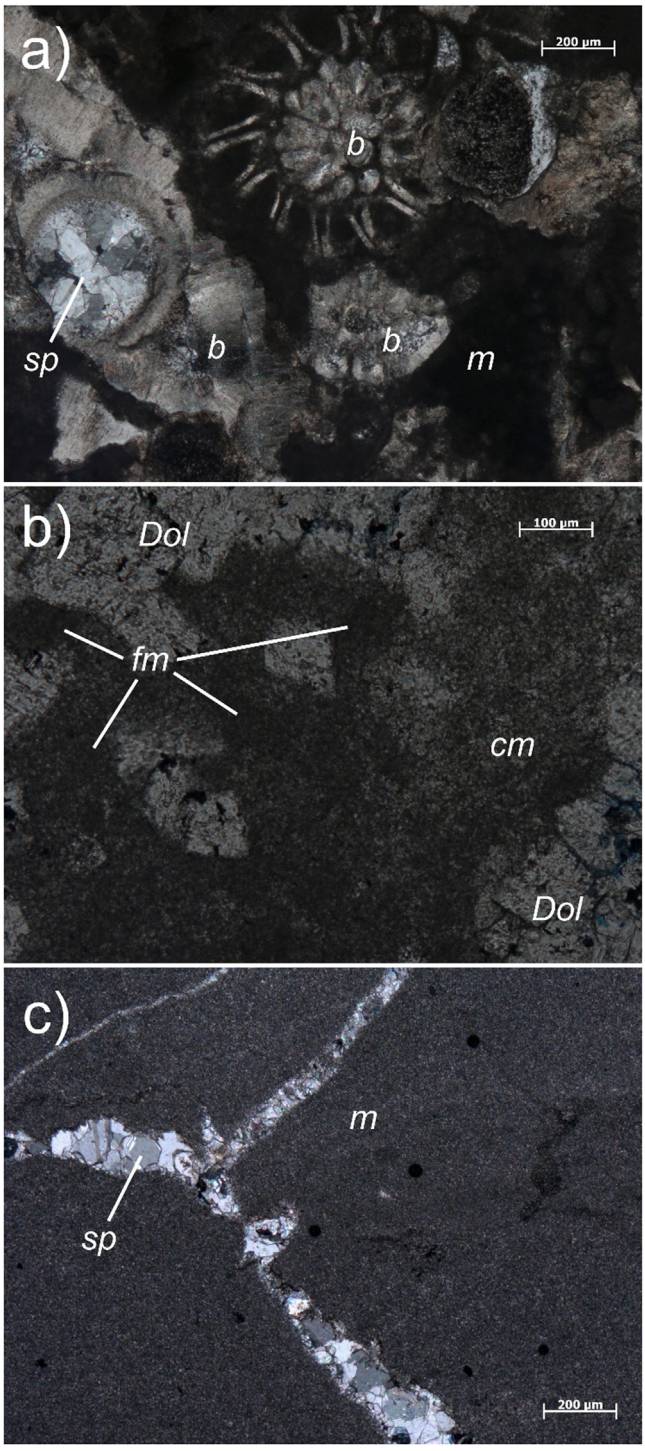

Fig. 1. Representative photomicrographs of thin sections under cross-polarised light: a) Typical textural elements of Chiampo Paglierino stone (5x) consisting in bioclasts (*b*), micrite domains (*m*) and foraminifera chambers filled by sparry calcite (*sp*); b) Botticino stone (10x) is characterized by domains made of fine-grained micrite (*fm*) and coarse-grained micrite (*cm*), containing abundant large dolomite crystals (*Dol*); c) Orsera stone (5x) is mainly made of micrite (*m*) with fenestrae and fractures sealed with sparry calcite (*sp*).

4. Results and discussion

4.1. Petrographic characterization

The results of the petrographic characterization, including information on the mineralogical composition, porosimetric properties, and density, are summarized in Table 2. Further information on the texture are also reported in Table 2, presenting the grain-size measurements performed on thin section under the optical microscope. Examples of the different textural elements (e.g. domains made of fine-grained micrite, coarse-grained micrite, sparry calcite, or bioclasts) characterized by different grain-size of the calcite crystals are reported in Fig. 1. We refer to Salvini and co-authors [96] for a detailed description of petrographic features, grain-size measurements and pore-size distribution.

Table 3
Average recession values (μm) calculated from weight loss measurements and measured from the analysis of 3D surface maps obtained by confocal microscopy after 54, 141 and 240 immersion cycles in the two types of water. Stone ID as in Table 1.

Stone ID	Bologna water						Stresa water					
	Weight loss			Confocal microscopy			Weight loss			Confocal microscopy		
Cycles	**54**	**141**	**240**	**54**	**141**	**240**	**54**	**141**	**240**	**54**	**141**	**240**
NA	3.50	10.19	14.3	–	8.20	14.30	6.40	13.46	20.4	13.72	–	26.89
CO	4.79	12.22	16.2	3.06	9.77	18.05	5.68	14.21	21.9	6.21	18.80	28.93
AU	3.35	8.72	11.3	6.42	14.12	17.03	8.73	15.91	21.7	8.49	18.87	33.00
OR	8.05	16.96	20.2	7.87	14.80	22.07	6.06	17.55	26.3	14.70	28.40	34.55
PA	4.80	11.31	13.9	6.19	–	15.69	6.05	14.09	20.6	7.44	21.91	31.78
ON	5.26	11.18	13.8	6.10	14.61	24.42	7.10	13.80	20.6	7.28	24.43	32.98
RV	6.03	12.83	15.7	5.29	14.81	–	4.84	11.58	21.3	9.48	23.46	28.47
BV	2.25	8.17	10.7	5.66	10.70	14.34	5.13	10.32	18.9	5.53	–	31.61
RO	4.81	9.72	12.5	–	–	16.90	10.28	18.31	24.6	10.14	20.92	31.38
BO	4.37	9.68	12.1	–	13.13	15.97	4.84	11.33	16.1	8.74	–	33.94
M	3.29	8.37	11.1	5.52	10.42	13.03	6.38	12.44	17.4	11.87	21.08	28.02

4.2. Surface recession

4.2.1. Experimental findings

The average recession values determined with the two different methods above described (i.e. calculated from the weight loss, and measured by confocal laser microscopy) are reported in Table 3.

Firstly, average recession resulted to be controlled by the water composition used during the ageing cycles; in particular, there is a clear relation with water pH, which is about 6 for that of Stresa and 7 for that of Bologna. Consequently, the samples immerged in the Stresa water, characterized by a lower pH, always show higher average values of recession.

Secondly, stones with markedly different textural characteristics, especially calcite grain-size, displayed significantly different recession values. For example, comparing two materials with similar (low) porosity and different grain-size of calcite crystals as the Carrara marble, characterized by a homogeneous coarse-grained texture (average calcite size of ~ 150 μm), and the Orsera stone, almost entirely made of micrite (very fine-grained calcite, with average size of ~ 0.5 μm), recession in the fine-grained Orsera stone is about 55% higher than in the coarse-grained Carrara marble. Aurisina stone shows intermediate recession values instead; although its grain-size is relatively coarse (average ~ 30 μm), it is still significantly finer than Carrara marble. Another illustrative case is represented by the recession of Botticino stone, which displayed average recession values similar to Aurisina stone, although calcite is almost entirely represented by micrite (average ~ 6 μm). This is readily explained considering that about 46% of the rock is made of dolomite, which is by far less soluble then calcite.

No evident correlation was found with porosity instead. For example, Costozza and Nanto stones, which have a porosity of about 28%, recorded an average recession significantly lower than Orsera stone, characterized by a porosity as low as 0.4%, and prevalently made of micrite. We may expect a positive correlation between recession rate and specific surface area. Instead, Orsera stone displayed a specific surface area orders of magnitude lower than Costozza and Nanto stones (Table 2). This incongruence may be only apparent, and related to the method used to calculate the surface area (i.e. applying the Rootare-Prenzlow equation to MIP data). This approach is reasonable when pores above 1 μm prevail, but probably underestimates the specific surface area when micro-pores are dominant. In addition, thermal shock during emersion and subsequent immersion may have increased the micro-porosity close to the surface, especially in fine-grained stones, thus locally increasing specific surface area well above the calculated one.

The analysis of the 3D surface maps obtained by confocal laser microscopy allowed to separately quantify surface recession in portions of the rock characterized by different textural features, such as those made of micrite respect to those made of sparry calcite, or bioclasts. Fig. 2 shows two representative 3D surface maps obtained by confocal laser microscopy on samples of Chiampo Paglierino stone and Botticino stone before and after the ageing test with Stresa water. In the case of Chiampo Paglierino stone, the evolution of the stone surface during the ageing test shows a clear differential recession of the bioclasts, which remain in relief in respect to the surrounding fine-grained micrite and the sparry calcite observed in veins or along bioclast rims. In the case of Botticino, the dolomite crystals markedly "rise" from the receding surrounding micrite; after 240 ageing cycles with the Stresa water, the dolomite shows an average recession of about 0.5 μm, while the micrite reaches values of about 33 μm (fine-grained portion) and 29 μm (coarse-grained portion), respectively.

From a general point of view, the topographic analysis of the 3D surface maps suggests that coarse-grained sparry calcite shows an average recession being around half of the recession of fine-grained micrite. Coarse-grained micrite shows values only slightly lower than those of fine-grained micrite. Finally, the bioclast recession covers a broad spectrum of values, which are often intermediate between those of sparry calcite and of coarse-grained micrite (Table 4). This further supports the observed direct control of grain-size on the recession rate. The relevant aggregated data are displayed in Fig. 3, showing clear correlation trends between recession and grain-size, the two trend lines and the relative equations referring to the recession in the water from Bologna and Stresa, respectively.

In order to determine the amount of rainfall corresponding to the 240 cycles carried out in the ageing experiments, recession was calculated using some of the equations available from the literature and described above, mostly modelled on marble weathering [41,57–60], considering the typical SO_2, NO_2, O_3 concentrations (4 μg/m^3, 40 μg/m^3, and 50 μg/m^3, respectively) in the atmosphere of Padua [98] where the experiments were carried out, SO_2 and NO_2 deposition velocity equal to 0.3 cm/s and 0.1 cm/s, respectively [41,[60]], time of wetting (0.3) and temperature (25 °C) imposed during the experiments, water pH (6 and 7) and SO_4^{2-} concentration (0.082 mmol/L and 0.035 mmol/L) corresponding to those of the waters of Stresa and Bologna, respectively.

The average recession of Carrara marble experimentally measured by its weight loss after 240 ageing cycles, was 17.4 μm and 11.1 μm in the Stresa and in the Bologna water, respectively (Table 3). These values turned out to be very similar to those calculated applying Delalieux's equation (the only equation considering also SO_4^{2-} concentration in the water), and normalized to 1 m of rainfall, i.e., 15.28 μm and 11.53 μm, respectively. This suggests that the 240 cycles in the experimental conditions previously described correspond to a rainfall of about 1 m in natural conditions

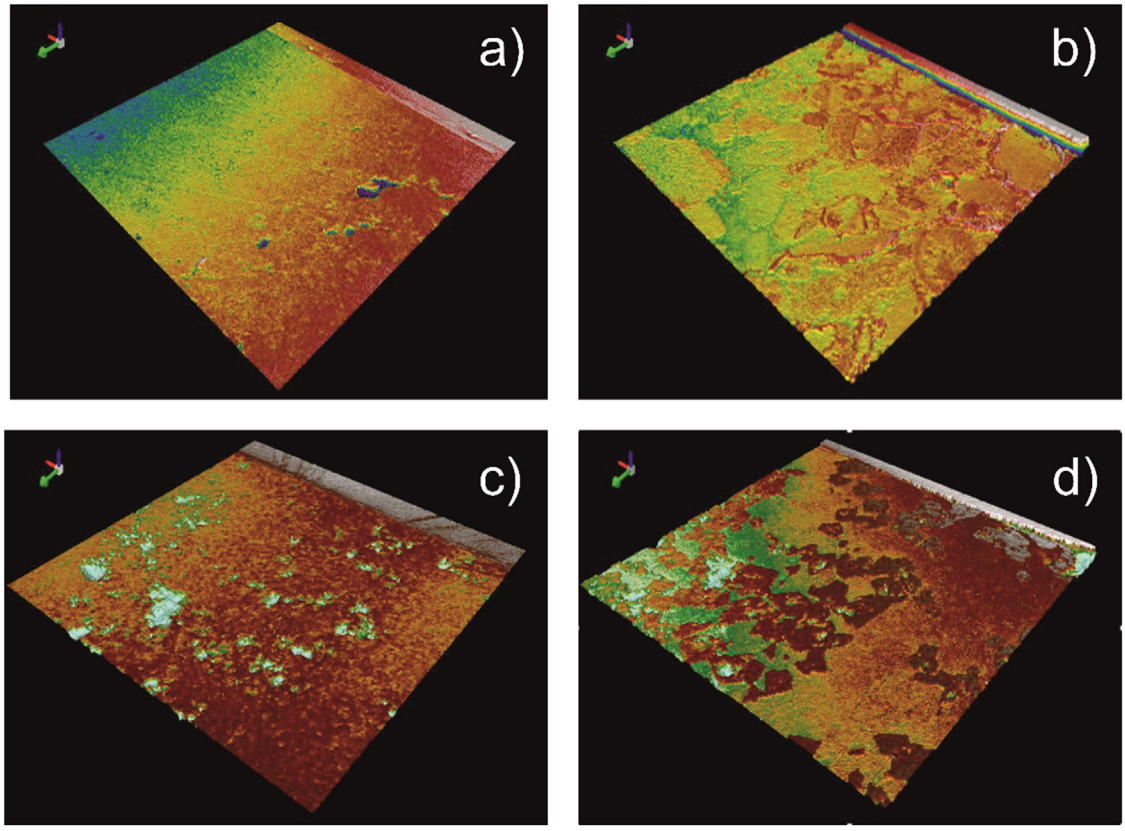

Fig. 2. 3D surface model of a sample of Chiampo Paglierino stone (a and b) and of Botticino stone (c and d) before the ageing test (left) and after 240 immersion cycles in the Stresa water (right). The side of the scanned area is about 3 mm. On the opposite side is the stainless still plate used as a reference in the evaluation of stone recession.

Table 4
Summary of the recession values (in µm) measured through the elaboration of the 3D models. Stone ID as in Table 1.

Stone ID	Fine-grained micrite		Coarse-grained micrite		Sparite		Bioclast filling		Dolomite	
	Bologna	Stresa	Bologna	Stresa	Bologna	Stresa	Bologna	Stresa	Bologna	Stresa
NA	20.36	32.86	10.67	–	5.73	17.17	13.06	24.37	–	–
CO	22.91	30.82	–	–	–	16.77	14.81	18.85	–	–
AU	22.23	40.77	18.51	–	11.36	20.23	13.64	26.94	–	–
OR	22.77	33.66	–	–	6.97	20.69	–	–	–	–
PA	21.54	36.80	17.42	–	10.5	17.55	13.64	26.33	–	–
ON	21.24	39.78	18.21	37.32	8.82	24.53	18.09	30.20	–	–
RV	–	29.98	–	–	–	–	–	21.73	–	–
BV	17.59	34.41	15.14	35.27	7.38	23.09	8.83	26.80	–	–
RO	19.15	34.10	16.54	–	–	–	11.31	20.61	–	–
BO	17.23	33.25	14.33	29.21	–	–	15.13	–	2.33	0.5
M	–	–	–	–	10.61	24.42	–	–	–	–
Mean	20.56	34.64	15.83	33.93	8.77	20.56	13.56	24.48	2.33	0.50

and exposure, that represents approximately the annual rainfall in numerous cities of northern Italy. Other equations gave less concordant results. Webb's and Lipfert's equations provided the highest recession values (~ 24.5 and 19.75 µm for both the waters, respectively), while Reddy's, Baedecker's, and Kucera's functions all gave considerably lower values, between 4.12 and 6.44 µm.

4.2.2. Correction coefficient

The dataset obtained during this study is useful for providing a broad perspective on stone recession considering together a number of petrographic parameters, that is, grain size, heterogeneity of grain-size distribution, content in clay minerals, porosity, etc. The global effects of these properties on stone recession are considered calculating a coefficient Φ, which is proposed for obtaining more reliable projections and predictive trends of stone deterioration for different types of carbonate rocks. The coefficient Φ is the ratio between the recession of a given stone material and the recession of Carrara Marble in the same ageing conditions (Table 5). Table 6 suggests other similar stone materials for which the coefficient might be used.

The applicability of the coefficient Φ calculated from the weight loss measurements was tested using the equation by Reddy and co-authors [57] to calculate stone recession for a number of different materials for which direct recession measurements are available in the literature, and average SO_2 and $[H^+]$ concentrations have been also provided [41]. Finally, the calculated recession was multiplied by the pertaining coefficient Φ and compared with the direct measures. Table 7 summarizes the relevant findings.

The coefficient Φ calculated for Nanto stone (1.23) was used to correct the recession values calculated for the Portland limestone in highly polluted and rural areas in the UK [99], and for a porous limestone exposed to a urban environment in Austria [100]; these

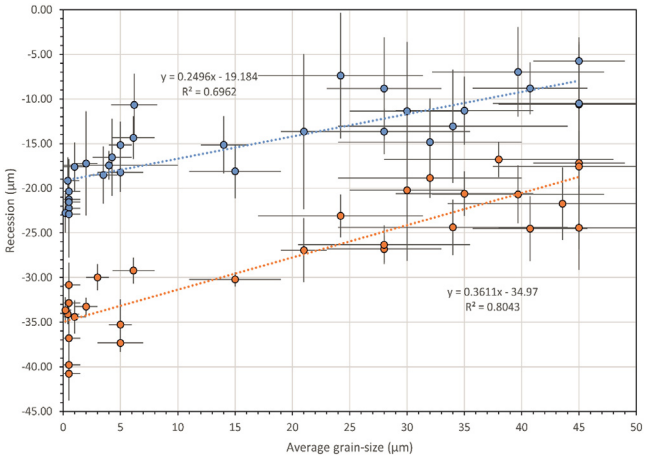

Fig. 3. Correlation between average grain size (accounting for the different textural elements and a representative range 0–45 µm) and average recession measured on all the samples after 240 ageing cycles with the water from Bologna (upper blue trend) and Stresa (lower orange trend).

Table 5
Average coefficient Φ calculated from the recession after 240 ageing cycles estimated by weight-loss measurements (WL) for the two types of water. Stone ID as in Table 1.

Stone ID	Bologna – WL		Stresa – WL		Mean Φ (WL)
	Recession	Φ	Recession	Φ	
NA	14.30	1.29	20.40	1.17	1.23
CO	16.20	1.46	21.90	1.26	1.36
AU	11.30	1.02	21.70	1.25	1.13
OR	20.20	1.82	26.30	1.51	1.67
PA	13.90	1.25	20.60	1.18	1.22
ON	13.80	1.24	20.60	1.18	1.21
RV	15.70	1.41	21.30	1.22	1.32
BV	10.70	0.96	18.90	1.09	1.03
RO	12.50	1.13	24.60	1.41	1.27
BO	12.10	1.09	16.10	0.93	1.01
M	11.10	1.00	17.40	1.00	1.00

materials display similar textural features if compared to Nanto stone in terms of calcite grain size, presence of bioclasts, porosity, and content in clay minerals. The coefficient Φ calculated for Botticino stone (1.01) indicates that average recession is similar to that observed in Carrara marble. Although recession in the micritic portion of this limestone is greater than in marble, the high content in dolomite of this rock reduces considerably the average recession value. For this reason, the same coefficient was applied to the Indiana limestone, which likewise has a noticeable dolomite content, low porosity and abundant micrite [57]. Furthermore, Chiampo stone is similar to a compact limestone studied by [100], in terms of texture and low porosity. For that, the correction coefficient Φ calculated for Chiampo stone (1.21) has been applied to that compact limestone.

With the exclusion of the Indiana limestone, for which the calculated recession value is higher than the measured one, in all the other cases the introduction of the correction coefficient provided recession estimates closer to the measured recession (Table 7). This suggests that the correction coefficient Φ in most of the cases sufficiently accounts for the different petrographic features influencing stone recession rate in the same environmental conditions. However, the application of such a coefficient does not always produce a perfect matching with measured data, hence the necessity for further investigations.

5. Conclusions

The previous research on stone weathering has proposed a number of mathematical relations for predicting or indirectly evaluating stone recession rate based on a set of environmental parameters, generally applied to marbles. However, those equations turn out to be less reliable when applied to limestones, which likewise have an immense importance from the perspective of usage and application in cultural heritage, including monumental sites, construction, and sculpture.

For further exploring this topic, an experimental investigation was conducted to determine the possible correlation between recession of different carbonate rocks used in the cultural heritage of northeastern Italy and their petrographic features. To that purpose, a series of ageing tests were done in an environmental test chamber simulating the effects of rain, with the same composition of rainwater in the two Italian cities of Bologna (water pH ~ 7) and Stresa (pH ~ 6).

Stone recession was calculated on the basis of material weight loss and measured by confocal microscopy, and correlated to calcite grain size: the finer the grain size, the faster the recession, independently from the contribution of environmental parameters. The novelty of this experimental approach is that recession was separately measured on portions of the stone surface characterized by different textural features, thus quantifying the recession related to grain size and water pH. The choice to prepare water compositions as similar as possible to real rainwater has been made to simulate the dissolution processes taking place between such waters and the stone surface. The limitation of this approach is that the range of water pH values in our experiments was relatively narrow. Nonetheless, the dissolution rate resulted significantly different in the two cases.

Based on the relevant datasets, a correction coefficient was calculated, to be applied for estimating the recession of other carbonate rocks with similar textural and mineralogical features. In this way, the durability and weathering risk of a wide variety of stones used in heritage artifacts and structures can be indirectly evaluated, possibly guiding the adoption of protection measures. Alter-

Table 6
Suggested coefficients Φ for various carbonate rocks based on the results presented in this study and calculated from the weight loss measurements. These values are also applicable to other stones characterized by similar mineralogical composition, texture, and grain size.

Stone	Petrographic classification	Φ	Porosity	Notes	Also suggested for
Carrara Marble	Crystalline carbonate	1.00	Low	Grain size ≈ 100 µm	Marbles from Naxos, Paros, Aghia Marina; Pentelico
Botticino Stone	Dolomitic Micrite/ Crystalline carbonate	1.01	Low	Cal 57%, Dol 43%	Indiana limestone
Verona Stone	Biomicrite Wackestone	1.03–1.32	Very Low	High heterogeneity, nodular limestone	Rouge du Roi, Tardos (Hungary), Adneter (Austria), Moneasa (Romania)
Chiampo Stone	Biomicrite/ Grainstone	1.21–1.22	Low		Rouge Languedoc Beige of Missolonghi
Vicenza Stone (Nanto)	Biomicrite/ Packstone	1.23	High	Micritized fossils, clay components, heterogeneity	Portland, Lecce, Noto

Table 7
Application of coefficients Φ (calculated from the weight loss measurements) to the recession estimates obtained using the equation of Reddy et al. [57], and comparison with measured recession rates (in μm). HP77: Honeyborne and Price [99]; R85: Reddy et al. [57]; W85: Weber [100].

Ref.	Location	Material	Measured recession	SO_2 (μg/m^3)	Rainfall (m/yr)	[H^+] (mmol/L)	Recession (R85)	Corrected rec. value	Φ
HP77	London	Portland	50.0	140	1	0.150	37.04	45.57	1.23
HP77	Rural, U.K.	Portland	17.0	30	1	0.015	9.20	11.32	1.23
R85	East U.S.	Indiana Limestone	7.5	20	1	0.015	8.51	8.58	1.01
W85	Vienna	Porous Limestone	26.5	70	1	0.055	17.96	22.10	1.23
W85	Vienna	Compact Limestone	20.1	70	1	0.055	17.96	21.80	1.21
W85	Vienna	Marble	18.0	70	1	0.055	17.96	17.96	1.00

natively, the same experimental approach could be used to evaluate the recession rate of a carbonate stone used in a specific historic building by using rainwater composition of that specific site.

Further investigations starting from this point are expected, also aimed at developing new theoretical relations encompassing both petrographic and environmental parameters at the same time.

Acknowledgement

This research was funded by the University of Padova (Project CPDA151883; C.M.) and by the HYPERION project. HYPERION has received funding from the European Union's Horizon 2020 research and innovation programme under grant agreement no 821054. The content of this publication is the sole responsibility of University of Padova, and does not necessarily reflect the opinion of the European Union.

References

[1] D. Camuffo, Physical weathering of stones, The Sci.Total Environ. 167 (1995) 1–14, doi:10.1016/0048-9697(95)04565-I.
[2] R. Altindag, I.S. Alyildiz, T. Onargan, Mechanical property degradation of ignimbrite subjected to recurrent freeze-thaw cycles, Int. J. Rock Mech. Min. Sci. 41 (6) (2004) 1023–1028, doi:10.1016/j.ijrmms.2004.03.005.
[3] K. Hall, Evidence for freeze-thaw events and their implications for rock weathering in northern Canada, Earth Surf Process and Landforms 29 (2004) 43–57, doi:10.1002/esp.1012.
[4] J.J. Beaudoin, C. MacInnis, The mechanism of frost damage in hardened cement paste, Cem. Concr. Res. 4 (1974) 139–147, doi:10.1016/0008-8846(74)90128-8.
[5] G.W. Scherer, J.J. Valenza, Mechanisms of frost damage, in: F. Young, J. Skalny (Eds.), Materials Science of concrete, VII, The American Ceramic Society, Westerville, 2005, pp. 209–246.
[6] C. Sabbioni, P. Brimblecombe, M. Cassar, The atlas of climate change impact on european cultural heritage, Scientific Analysis and Management Strategies, Anthem Press, London, 2010, doi:10.2777/11959.
[7] K. Zehnder, A. Arnold, Crystal growth in salt efflorescence, J. Cryst. Growth 97 (2) (1989) 513–521, doi:10.1016/0022-0248(89)90234-0.
[8] R. Rossi-Manaresi, A. Tucci, Pore structure and the disruptive or cementing effect of salt crystallisation in various types of stone, Stud. Conserv. 36 (1991) 53–58, doi:10.1179/sic.1991.36.1.53.
[9] D. Benavente, M.A. García del Cura, R. Fort, S. Ordóñez, Thermodynamic modelling of changes induced by salt pressure crystallisation in porous media of stone, J. Cryst. Growth 204 (1999) 168–178, doi:10.1016/S0022-0248(99)00163-3.
[10] G.W. Scherer, Crystallization in pores, Cem. Concr. Res. 29 (8) (1999) 1347–1358, doi:10.1016/S0008-8846(99)00002-2.
[11] G.W. Scherer, Stress from crystallization of salt, Cem. Concr. Res. 34 (9) (2004) 1613–1624, doi:10.1016/j.cemconres.2003.12.034.
[12] R.J. Flatt, Salt damage in porous materials: how high supersaturations are generated, J. Cryst. Growth 242 (2002) 435–454, doi:10.1016/S0022-0248(02)01429-X.
[13] M. Steiger, Crystal growth in porous materials I: the crystallization pressure of large crystals, J. Cryst. Growth 282 (2005) 455–469 a, doi:10.1016/j.jcrysgro.2005.05.007.
[14] M. Steiger, Crystal growth in porous materials II: influence of crystal size on the crystallization pressure, J. Cryst. Growth 282 (2005) 470–481 b, doi:10.1016/j.jcrysgro.2005.05.008.
[15] A. Moropoulou, P. Theoulakis, T. Chrysophakis, Correlation between stone weathering and environmental factors in marine atmosphere, Atmos. Environ. 29 (8) (1995) 895–903, doi:10.1016/1352-2310(94)00322-C.
[16] F. Zezza, F. Macrì, Marine aerosol and stone decay, Sci. Total Environ. 167 (1995) 123–143, doi:10.1016/0048-9697(95)04575-L.
[17] K. Torfs, R. Van Grieken, Chemical relations between atmospheric aerosols, deposition and stone decay layers on historic buildings at the Mediterranean coast, Atmos. Environ. 31 (1997) 2179–2192, doi:10.1016/S1352-2310(97)00038-1.
[18] A. Chabas, D. Jeannette, Weathering of marbles and granites in marine environment: petrophysical properties and special role of atmospheric salts, Environ. Geol. 40 (3) (2001) 359–368, doi:10.1007/s002540000157.
[19] C. Cardell, F. Delalieux, K. Roumpopoulos, A. Moropoulou, F. Auger, R. Van Grieken, Salt-induced decay in calcareous stone monuments and buildings in a marine environment in SW France, Constr. Build. Mater. 17 (3) (2003) 165–179, doi:10.1016/S0950-0618(02)00104-6.
[20] D. Camuffo, Condensation-evaporation cycles in pore and capillary systems according to the Kelvin model, Water Air Soil Pollut. 21 (1) (1984) 151–159, doi:10.1007/BF00163620.
[21] D. Camuffo, G. Sturaro, The climate of Rome and its action on monument decay, Climate Res. 16 (2001) 145–155, doi:10.3354/cr016145.
[22] E. Zendri, G. Biscontin, P. Kosmidis, Effects of condensed water on limestone surfaces in a marine environment, J. Cult. Herit. 2 (4) (2001) 283–289, doi:10.1016/S1296-2074(01)01132-3.
[23] R.D. Wakefield, M.S. Jones, An introduction to stone colonizing microorganisms and biodeterioration of building stone, Q. J. Eng. Geol. Hydrogeol. 31 (4) (1998) 301–313, doi:10.1144/GSL.QJEG.1998.031.P4.03.
[24] T. Warscheid, J. Braams, Biodeterioration of stone: a review, Int. Biodeterior. Biodegrad. 46 (4) (2000) 343–368, doi:10.1016/S0964-8305(00)00109-8.
[25] E. Zanardini, P. Abbruscato, N. Ghedini, M. Realini, C. Sorlini, Influence of atmospheric pollutants on the biodeterioration of stone, Int. Biodeterior. Biodegrad. 45 (2000) 35–42, doi:10.1016/S0964-8305(00)00043-3.
[26] C. Urzì, L. Brusetti, P. Salamone, C. Sorlini, E. Stackebrandt, D. Daffonchio, Biodiversity of Geodermatophilaceae isolated from altered stones and monuments in the Mediterranean basin, Environ. Microbiol. 3 (7) (2001) 471–479, doi:10.1046/j.1462-2920.2001.00217.x.
[27] M. Lisci, M. Monte, E. Pacini, Lichens and higher plants on stone: a review, Int. Biodeterior. Biodegrad. 51 (1) (2003) 1–17, doi:10.1016/S0964-8305(02)00071-9.
[28] D. Camuffo, Acid rain and deterioration of monuments: how old is the phenomenon? Atmos. Environ. Part B Urban Atmos. 26 (2) (1992) 241–247, doi:10.1016/0957-1272(92)90027-P.
[29] P.A. Baedecker, M.M. Reddy, The erosion of carbonate stone by acid rain, J. Chem. Educ. 70 (2) (1993) 104–108, doi:10.1021/ed070p104.
[30] H.A. Bravo, R.A. Soto, R.M.I. Saavedra, R.J. Torres, L.M.M. Granada, P.A. Sánchez, Acid rain in Mexico case: maya monuments, WIT Trans. Ecol. Environ. 21 (1998) 661–674, doi:10.2495/AIR980641.
[31] W. Marquardt, E. Brüggemann, R. Auel, H. Herrmann, D. Möller, Trends of pollution in rain over East Germany caused by changing emissions, Tellus B Chem. Phys. Meteorol. 53 (5) (2001) 529–545, doi:10.3402/tellusb.v53i5.16631.
[32] A. Singh, M. Agrawal, Acid rain and its ecological consequences, J. Environ. Biol. 29 (1) (2008) 15–24 PMID: 18831326.
[33] S. Reis, P. Grennfelt, Z. Klimont, M. Amann, H. ApSimon, J.-.P. Hettelingh, M. Holland, A.-.C. LeGall, R. Maas, M. Posch, T. Spranger, M.A. Sutton, M. Williams, From acid rain to climate change, Science 338 (2012) 1153–1154, doi:10.1126/science.1226514.
[34] R.J. Charlson, H. Rodhe, Factors controlling the acidity of natural rainwater, Nature 295 (1982) 683–685, doi:10.1038/295683a0.
[35] J.G. Dikaiakos, C.G. Tsitouris, P.A. Siskos, D.A. Melissos, P. Nastos, Rainwater composition in Athens, Greece, Atmos. Environ. Part B Urban Atmos. 24 (1) (1990) 171–176, doi:10.1016/0957-1272(90)90022-m.
[36] C. Samara, R. Tsitouridou, C. Balafoutis, Chemical composition of rain in Thessaloniki, Greece, in relation to meteorological conditions, Atmos. Environ. Part B Urban Atmos. 26 (3) (1992) 359–367, doi:10.1016/0957-1272(92)90011-G.
[37] C. Cardell-Fernández, G. Vleugels, K. Torfs, R. Van Grieken, The processes dominating Ca dissolution of limestone when exposed to ambient atmospheric conditions as determined by comparing dissolution models, Environ. Geol. 43 (1) (2002) 160–171, doi:10.1007/s00254-002-0640-x.
[38] A. Bonazza, P. Messina, C. Sabbioni, C.M. Grossi, P. Brimblecombe, Mapping the impact of climate change on surface recession of carbonate buildings in Europe, Sci. Total Environ. 407 (6) (2009) 2039–2050, doi:10.1016/j.scitotenv.2008.10.067.
[39] E. Franzoni, E. Sassoni, Correlation between microstructural characteristics and weight loss of natural stones exposed to simulated acid rain, Sci. Total Environ. 412 (2011) 278–285, doi:10.1016/j.scitotenv.2011.09.080.

[40] K. Lal Gauri, G.C. Holdren Jr., Pollutant effects on stone monuments, Environ. Sci. Technol. 15 (4) (1981) 386–390, doi:10.1021/es00086a001.
[41] F.W. Lipfert, Atmospheric damage to calcareous stones: comparison and reconciliation of recent experimental findings, Atmos. Environ. 23 (1989) 415–429, doi:10.1016/0004-6981(89)90587-8.
[42] D.A. Dolske, Deposition of atmospheric pollutants to monuments, statues, and buildings, Sci. Total Environ. 167 (1–3) (1995) 15–31, doi:10.1016/0048-9697(95)04566-J.
[43] D.E. Searle, D.J. Mitchell, The effect of coal and diesel particulates on the weathering loss of Portland Limestone in an urban environment, Sci. Total Environ. 370 (2006) 207–223, doi:10.1016/j.scitotenv.2006.07.005.
[44] E.S. McGee, V.G. Mossotti, Gypsum accumulation on carbonate stone, Atmos. Environ. Part B Urban Atmos. 26 (2) (1992) 249–253, doi:10.1016/0957-1272(92)90028-Q.
[45] V. Fassina, M. Favaro, A. Naccari, Principal decay patterns on Venetian monuments, in: S. Siegesmund, T. Weiss, A. Vollbrecht (Eds.), Natural stone, Weathering phenomena, Conservation Strategies and Case Studies, Geological Society, London, 2002, pp. 381–391, doi:10.1144/GSL.SP.2002.205.01.27. Special Publications 205.
[46] C. Sabbioni, N. Ghedini, A. Bonazza, Organic anions in damage layers on monuments and buildings, Atmos. Environ. 37 (9) (2003) 1261–1269, doi:10.1016/S1352-2310(02)01025-7.
[47] C.M. Grossi, P. Brimblecombe, A. Bonazza, C. Sabbioni, J. Zamagni, Sulfate and carbon compounds in black crusts from the Cathedral of Milan and Tower of London, in: R. Fort, M. Alvarez de Buergo, M. Gomez-Heras, C. Vazquez–Calvo (Eds.), Proceedings of the International Heritage, Weathering and Conservation Conference (HWC-2006), Madrid, Spain, CRC Press, 2006 21-24 June 2006.
[48] P. Brimblecombe, Air Composition and Chemistry, Cambridge University Press, 1996.
[49] C. Varotsos, C. Tzanis, A. Cracknell, The enhanced deterioration of the cultural heritage monuments due to air pollution, Environ. Sci. Pollut. Res. 16 (2009) 590–592, doi:10.1007/s11356-009-0114-8.
[50] M. Giugliano, G. Lonati, P. Butelli, L. Romele, R. Tardivo, M. Grosso, Fine particulate (PM2.5–PM1) at urban sites with different traffic exposure, Atmos. Environ. 39 (13) (2005) 2421–2431, doi:10.1016/j.atmosenv.2004.06.050.
[51] G. Lonati, M. Giugliano, P. Butelli, L. Romele, R. Tardivo, Major chemical components of PM2.5 in Milan (Italy), Atmos. Environ. 39 (10) (2005) 1925–1934, doi:10.1016/j.atmosenv.2004.12.012.
[52] R.M. Esbert, F. Dıaz-Pache, C.M. Grossi, F.J. Alonso, J. Ordaz, Airborne particulate matter around the Cathedral of Burgos (Castilla y León, Spain), Atmos. Environ. 35 (2) (2001) 441–452, doi:10.1016/S1352-2310(00)00113-8.
[53] P. Brimblecombe, C.M. Grossi, Millennium long damage to building materials in London, Sci. Total Environ. 407 (4) (2009) 1354–1361, doi:10.1016/j.scitotenv.2008.09.037.
[54] P. Brimblecombe, C.M. Grossi, Millennium long recession of limestones facades in London, Environ. Geol. 56 (2008) 463–471, doi:10.1007/s00254-008-1465-z.
[55] C.M. Grossi, A. Bonazza, P. Brimblecomble, I. Harris, C. Sabbioni, Predicting twenty-first century recession of architectural limestone in European cities, Environ. Geol. 56 (2008) 455–461, doi:10.1007/s00254-008-1442-6.
[56] R.J. Inkpen, Reconstructing past atmospheric pollution levels using gravestone erosion rates, Area 45 (3) (2013) 321–329, doi:10.1111/area.12035.
[57] M.M. Reddy, S. Sherwood, B. Doe, Limestone and marble dissolution by acid rain, in: 5th Int. Congress on Conservation and Deterioration of Stone, Lausanne, 1985, pp. 517–526.
[58] P.A. Baedecker, Dose-response functions for the chemical erosion of carbonate stone, in: Effects of Acidic Deposition On Materials, National Acidic Precipitation Assessment Program, Washington, D.C., 1990, p. 123. NAPAP Report 19 on Acidic Deposition: State of Science and Technology.
[59] F. Delalieux, C. Cardell-Fernandez, K. Torfs, G. Vleugels, R. Van Grieken, Damage functions and mechanism equations derived from limestone weathering in field exposure, Water, Air, Soil Pollut. 139 (1) (2002) 75–94, doi:10.1023/A:1015827031669.
[60] A.H. Webb, R.J. Bawden, A.K. Busby, J.N. Hopkins, Studies on the effects of air pollution on limestone degradation in Great Britain, Atmos. Environ. Part B Urban Atmos. 26 (2) (1992) 165–181, doi:10.1016/0957-1272(92)90020-S.
[61] V. Kucera, S. Fitz, Direct and indirect air pollution effects on materials including cultural monuments, Water Air Soil Pollut. 85 (1995) 153–165, doi:10.1007/BF00483697.
[62] J. Tidblad, V. Kucera, A.A. Mikhailov, J. Henriksen, K. Kreislova, T. Yates, UN ECE ICP materials: dose-response functions on dry and wet acid deposition effects over 8 years of exposure, Water Air Soil Pollut. 130 (2001) 1457–1462, doi:10.1023/A:1013965030909.
[63] MULTI-ASSESS, Model for multi-pollutant impact and assessment of threshold levels for cultural heritage, Deliverable 02, 2007.
[64] V. Kucera, J. Tidblad, K. Kreislova, D. Knotkova, M. Faller, R. Reiss, R. Snethlage, T. Yates, J. Henriksen, M. Schreiner, M. Melcher, M. Ferm, R.-A. Lefèvre, J. Kobus, UN/ECE ICP Materials Dose-response functions for the multi pollutant situation, Acid Rain Depos. Recov. (2007) 249–258.
[65] T.T.N. Lan, N.T.P. Thoa, R. Nishimura, Y. Tsujino, M. Yokoi, Y. Maeda, New model for the sulfation of marble by dry deposition Sheltered marble—The indicator of air pollution by sulfur dioxide, Atmos. Environ. 39 (5) (2005) 913–920, doi:10.1016/j.atmosenv.2004.09.074.
[66] R.A. Livingston, Acid rain attack on outdoor sculpture in perspective, Atmos. Environ. 146 (2016) 332–345, doi:10.1016/j.atmosenv.2016.08.029.
[67] V. Comite, M. Álvarez de Buergo, D. Barca, C.M. Belfiore, A. Bonazza, M.F. La Russa, A. Pezzino, L. Randazzo, S.A. Ruffolo, Damage monitoring on carbonate stones: field exposure tests contributing to pollution impact evaluation in two Italian sites, Constr. Build. Mater. 152 (2017) 907–922, doi:10.1016/j.conbuildmat.2017.07.048.
[68] R.J. Inkpen, H. Viles, C. Moses, B. Baily, Modelling the impact of changing atmospheric pollution levels on limestone erosion rates in central London, 1980-2010, Atmos. Environ. 61 (2012) 476–481 a, doi:10.1016/j.atmosenv.2012.07.042.
[69] R.J. Inkpen, H. Viles, C. Moses, B. Baily, C. Collier, S.T. Trudgill, R.U. Cooke, Thirty years of erosion and declining atmospheric pollution at St Paul's Cathedral, London, Atmos. Environ. 62 (2012) 521–529 b, doi:10.1016/j.atmosenv.2012.08.055.
[70] M. Kottek, J. Grieser, C. Beck, B. Rudolf, F. Rubel, World Map of the Köppen-Geiger climate classification updated, Meteorol. Z. 15 (3) (2006) 259–263, doi:10.1127/0941-2948/2006/0130.
[71] P. Brimblecombe, Air pollution and society, EPJ Web Conf. 9 (2010) 227–232, doi:10.1051/epjconf/201009018.
[72] M.J. Thornbush, H.A. Viles, Simulation of the dissolution of weathered versus unweathered limestone in carbonic acid solutions of varying strength, Earth Surf. Process. Landforms 32 (6) (2007) 841–852, doi:10.1002/esp.1441.
[73] L. Herngren, A. Goonetilleke, R. Sukpum, D.D. Silva, Rainfall simulation as a tool for urban water quality research, Environ. Eng. Sci. 22 (3) (2005) 378–383, doi:10.1089/ees.2005.22.378.
[74] M.J. Melo, S. Bracci, M. Camaiti, O. Chiantore, P. Piacenti, Photodegradation of acrylic resins used in the conservation of stone, Polym. Degrad. Stab. 66 (1) (1999) 23–30, doi:10.1016/S0141-3910(99)00048-8.
[75] B. Dal Bianco, R. Bertoncello, A. Bouquillon, J. Dran, R. Milanese, S. Roehrs, C. Sada, J. Salomon, S. Voltolina, Investigation on sol-gel silica coatings for the protection of ancient glass: interaction with glass surface and protection efficiency, J. Non Cryst. Solids 354 (26) (2008) 2983–2992, doi:10.1016/j.jnoncrysol.2007.12.004.
[76] S. Salvini, B. Sacchi, P. Frediani, Study of protectives obtained from natural resources for the conservation of stone, in: Proceedings of the 28th International Conference "Scienza e Beni Culturali", Bressanone, 2012, pp. 833–843. 10 July 2012.
[77] C.D. Vacchiano, L. Incarnato, P. Scarfato, D. Acierno, Conservation of tuff-stone with polimeric resins, Constr. Build. Mater. 22 (5) (2008) 855–865, doi:10.1016/j.conbuildmat.2006.12.012.
[78] E.M. Winkler, Weathering and weathering rates of natural stone, Environ. Geol. Water Sci. 9 (1987) 85–92, doi:10.1007/BF02449939.
[79] G.G. Amoroso, V. Fassina, Stone Decay and conservation: Atmospheric pollution, cleaning, Consolidation and Protection, Elsevier, Amsterdam, 1983.
[80] S.T. Trudgill, H.A. Viles, R.J. Inkpen, R.U. Cooke, in: Remeasurement of Weathering Rates, 14, Earth Surface Processes and Landforms, St Paul's Cathedral, London, 1989, pp. 175–196, doi:10.1002/esp.3290140302.
[81] T.C. Meierding, Marble tombstone weathering rates: a transect of the United States, Phys. Geogr. 2 (1) (1981) 1–18, doi:10.1080/02723646.1981.10642201.
[82] N.S. Baer, S.M. Berman, Marble tombstone in national cemeteries as indicators of stone damage: general methods, in: Proceedings of the 76th Annual Meeting of the Air Pollution Control Association, 1983 June 19-24.
[83] J.J. Feddema, T.C. Meierding, Marble weathering and air pollution in Philadelphia, Atmos. Environ. 21 (1) (1987) 143–157, doi:10.1016/0004-6981(87)90279-4.
[84] S.M. Roberts, Surface-recession weathering of marble tombstones: new field data and constraints, in: A.V. Turkington (Ed.), Stone Decay in the Architectural Environment, Geological Society of America, 2005, pp. 27–37, doi:10.1130/0-8137-2390-6.27. Special Papers 390.
[85] D. Dragovich, Marble weathering in an industrial environment, Eastern Australia, Environ. Geol. Water Sci. 17 (2) (1991) 127–132, doi:10.1007/BF01701568.
[86] M.M. Reddy, Acid rain damage to carbonate stone: a quantitative assessment based on the aqueous geochemistry of rainfall runoff from stone, Earth Surf. Process. Landforms 13 (1988) 335–354, doi:10.1002/esp.3290130406.
[87] C.A. Moses, Methods for assessing stone decay mechanisms in polluted and 'clean' environments, in: B.J. Smith, P.A. Warke (Eds.), Processes of Urban Stone Decay, Donhead, Northern Ireland, 1996, pp. 212–227. ISBN 9781873394205.
[88] R.J. Inkpen, Stone decay and atmospheric pollution in a transect across southern Britain Unpublished PhD thesis, University of London, 1989.
[89] J. Lundberg, A. Ginés, Rillenkarren, in: A. Ginés, M. Knez, T. Slabe, W. Dreybrodt (Eds.), Karst Rock features, Karren sculpturing, Zalozba Z.R.C., Ljubljana, 2009, pp. 185–210.
[90] H.A. Viles, Microbial geomorphology: a neglected link between life and landscape, Geomorphology 129 (2011) 167–182, doi:10.1016/j.geomorph.2011.03.021.
[91] H.A. Viles, L.A. Naylor, N.E.A. Carter, D. Chaput, Biogeomorphological disturbance regimes: progress in linking ecological and geomorphological systems, Earth Surf. Process. Landforms 33 (9) (2008) 1419–1435, doi:10.1002/esp.1717.
[92] R.U. Cooke, Geomorphological contribution to acid rain research: studies of stone weathering, Geogr. J. 155 (1989) 361–366, doi:10.2307/635211.
[93] P. Panettiere, G. Cortecci, E. Dinelli, A. Bencini, M. Guidi, Chemistry and sulfur isotopic composition of precipitation at Bologna, Italy, Appl. Geochem. 15 (10) (2000) 1455–1467, doi:10.1016/S0883-2927(00)00012-3.
[94] M. Rogora, R. Mosello, A. Marchetto, Long-terms trends in the chemistry of

atmospheric deposition in Northwestern Italy: the role of increasing Saharan dust deposition, Tellus B Chem. Phys. Meteorol. 56 (2004) 426–434, doi:10.3402/tellusb.v56i5.16456.

[95] R. Pozzobon, C. Mazzoli, S. Salvini, F. Sauro, M. Massironi, T. Santagata, A DEM-based volume extraction approach: from micro-scale weathering forms to planetary lava tubes, in: A. Bistacchi, M. Massironi, S. Viseur (Eds.), 3D Digital Geological Models, John Wiley & Sons Ltd, 2022, pp. 133–147, doi:10.1002/9781119313922.ch8.

[96] S. Salvini, C. Coletti, L. Maritan, M. Massironi, A. Pieropan, R. Spiess, C. Mazzoli (submitted) Petrographic characterization and durability of carbonate stones used in UNESCO World Heritage sites in northeastern Italy. Environ. Earth Sci..

[97] H.M. Rootare, C.F. Prenzlow, Surface areas from mercury porosimetry measurements, J. Phys. Chem. 71 (8) (1967) 2733–2736, doi:10.1021/j100867a057.

[98] M. Masiol, S. Squizzato, G. Formenton, R.M. Harrison, C. Agostinelli, Air quality across a European hotspot: spatial gradients, seasonality, diurnal cycles and trends in the Veneto region, NE Italy, Sci. Total Environ. 576 (2017) 210–224, doi:10.1016/j.scitotenv.2016.10.042.

[99] D.B. Honeyborne, C.A. Price, Air pollution and the decay of limestone, Building Research Establishment Note 117/77, Garston, 1977.

[100] J. Weber, Natural and artificial weathering of Austrian building stones due to air pollution, in: Proceedings of the 5th International Congress on Deterioration and Conservation of Stone, Lausanne, 1985, pp. 527–535. Lausanne, 25-27 September 1985. Presses polytechniques romandes.